

This is the **accepted version** of the journal article:

Álvarez Prada, Luis Ignacio; Nguyen, Anh Dung; Romero Fernández, Nuria; [et al.]. «Insights into the light-driven hydrogen evolution reaction of mesoporous graphitic carbon nitride decorated with Pt or Ru nanoparticles». Dalton transactions, Vol. 51, issue 2 (January 2022), p. 731-740. DOI 10.1039/d1dt03006j

This version is available at <https://ddd.uab.cat/record/288211>

under the terms of the  ^{IN} COPYRIGHT license

ARTICLE

Insights into the light-driven hydrogen evolution reaction of mesoporous graphitic carbon nitride decorated with Pt or Ru nanoparticles

Received 00th January 20xx,
Accepted 00th January 20xx

DOI: 10.1039/x0xx00000x

Ignacio Álvarez-Prada,^a Anh Dung Nguyen,^b Nuria Romero,^a Heting Hou,^a Elisabetta Benazzi,^{c,‡} Lluís Escriche,^a Amitava Acharjya,^d Arne Thomas,^d Michael Schwarze,^b Reinhard Schomäcker,^b Xavier Sala,^a Mirco Natali,^{*c} Jordi García-Antón,^{*a} and Minoo Tasbihi^{*b}

Ru or Pt nanoparticles have been prepared following the organometallic approach and deposited onto the surface of mesoporous graphitic carbon nitride (mpg-CN). Three different Ru-based samples have been also compared to investigate the effect of 4-phenylpyridine as stabilizing agent. The photocatalytic performance towards the hydrogen evolution reaction (HER) has been tested showing that all hybrid systems clearly outperform the photocatalytic activity of bare mpg-CN. In particular, Pt-decorated mpg-CN yields the largest H₂ production upon visible-light irradiation (870 μmol·h⁻¹·g⁻¹, TOF = 14.1 h⁻¹, TON = 339 after 24 h) when compared with the Ru-based samples (137-155 μmol·h⁻¹·g⁻¹, TOFs between 2.3-2.7 h⁻¹, TONs between 54-57 after 24 h). Long-term photochemical tests (up to 65 h irradiation) show also an improved stability of the Pt-based samples over the Ru counterpart. Photophysical experiments aimed at rationalizing the photocatalytic performance of the different hybrid systems elucidate that the enhanced activity of the Pt-decorated mpg-CN over the Ru-based analogues arises from improved electron transfer kinetics from the mpg-CN to the metal nanoparticles.

Introduction

To address climate change, obtaining a carbon-free fuel is mandatory. In this context, hydrogen production through the sunlight-triggered photocatalytic water-splitting reaction is one of the most desirable options. If photocatalytic production and storage/transportation of hydrogen becomes cost-competitive, it will be a serious and clean competitor to fossil fuels.^{1,2} Water splitting can be divided into two half-reactions, namely the oxygen evolution reaction (OER) and the hydrogen evolution reaction (HER). It is important to note that an adequate catalyst for the overall water splitting reaction or a combination of two catalysts for the two half-reactions is needed to obtain acceptable reaction rates.³⁻⁵

For photocatalytic HER, a photoabsorber with the appropriate bandgap to harvest (sun)light must be excited leading to

accumulation of electrons in the conduction band (CB) and holes in the valence band (VB). The former can be exploited to catalytically reduce protons into hydrogen,⁶⁻⁸ while the latter can be used to oxidize a suitable electron donor. Graphitic carbon nitride is an adequate candidate as a photoabsorber, but needs to be coupled with a co-catalyst to facilitate the reaction, which otherwise is too slow due to undesired recombination between photogenerated electrons and holes.⁹⁻¹³ At present, platinum is the state-of-the-art co-catalyst for HER reaching the highest activities at relatively low concentrations.^{14,15} Nevertheless, its instability in basic media¹⁶ together with its high cost prompt to find a substitute. In this regard, Ru nanoparticles have been recently proved to be good candidates: they present high activity for the hydrogen evolution reaction and high stability in both acidic and basic media.¹⁷

To rationally elucidate the physical and chemical properties of nanomaterials and correlate them to their respective catalytic performances, it is mandatory to prepare such compounds through a reproducible synthetic methodology that can control their size, shape, structure, and surface environment. The so-called organometallic approach is a suitable and reproducible procedure to obtain metallic nanoparticles which are monodisperse in size and with a controlled surface environment. This approach consists in the decomposition of an organometallic precursor under mild conditions (typically room temperature and 3 bar of H₂) in the presence of a stabilizing agent.¹⁸ These stabilizing agents, which are typically organic ligands, allow to fine-tune the catalytic activity of the nanoparticles.¹⁹

^a Departament de Química, Unitat de Química Inorgànica, Universitat Autònoma de Barcelona, 08193 Bellaterra, Barcelona, Spain.

E-mail: Jordi.GarciaAnton@uab.es

^b Department of Chemistry, Technische Universität Berlin, Straße des 17. Juni, 10623 Berlin, Germany.

E-mail: minoo.tasbihi@tu-berlin.de

^c Dipartimento di Scienze Chimiche, Farmaceutiche ed Agrarie (DOCPAS), Università degli Studi di Ferrara, Via L. Borsari, 46, 44121 Ferrara, Italy.

E-mail: mirco.natali@unife.it

^d Department of Chemistry: Functional Materials, Technische Universität Berlin, 10623 Berlin, Germany.

‡ Current address: Dipartimento di Scienze Chimiche, Università di Padova, via F. Marzolo 1, 35131 Padova, Italy.

Electronic Supplementary Information (ESI) available: characterization data, hydrogen evolution kinetics, photophysical data. See DOI: 10.1039/x0xx00000x

In the present work, a new set of hybrid materials composed of mesoporous graphitic carbon nitride (mpg-CN) as photoabsorber coupled to Ru or Pt nanoparticles (NPs), obtained via the above-mentioned organometallic approach, has been prepared and tested in the photocatalytic hydrogen evolution reaction. The effect of 4-phenylpyridine as stabilizing agent of the Ru NPs has been also examined. The different performances of the hybrid systems experimentally observed have been finally addressed by means of photophysical experiments.

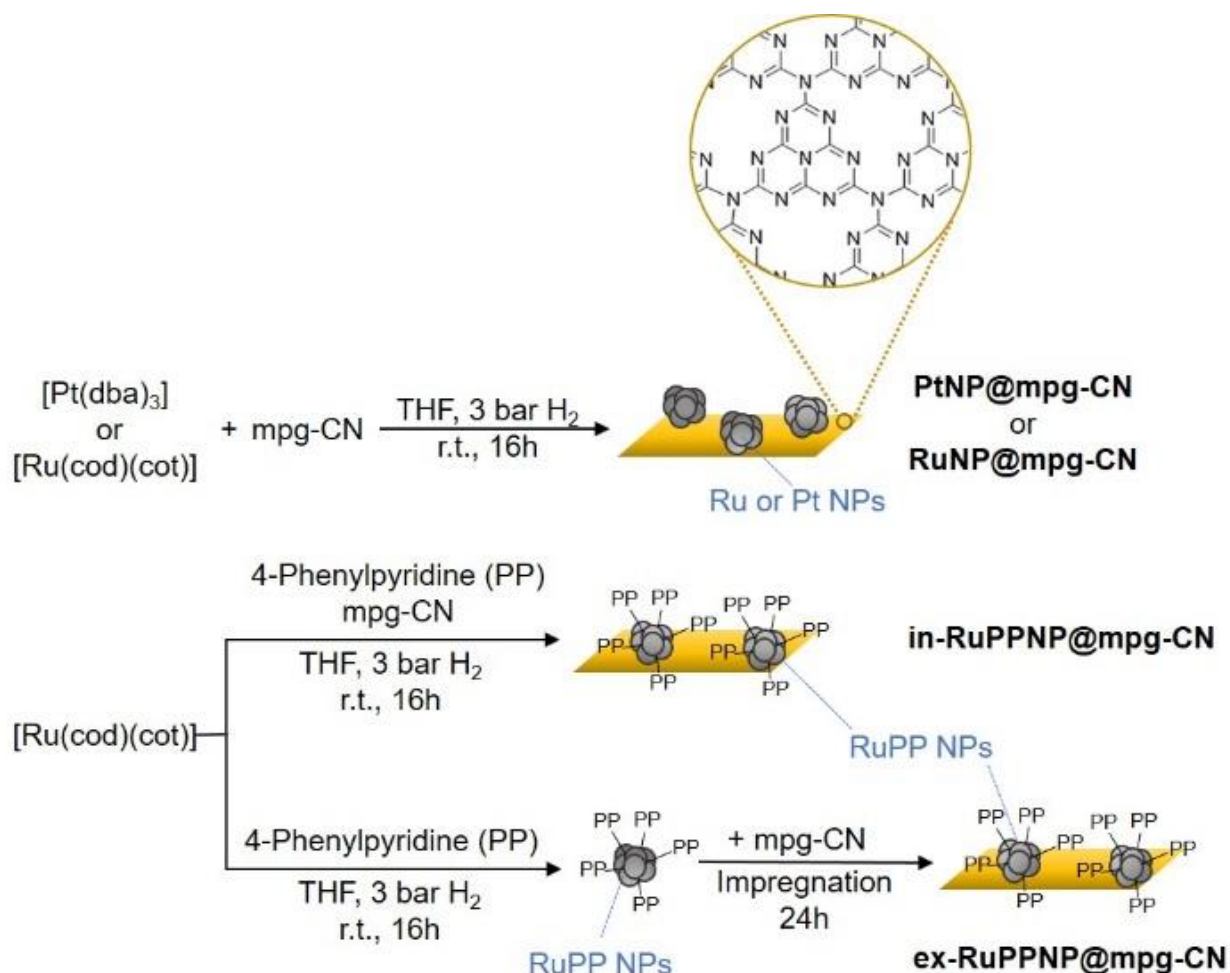
Results

Synthesis and characterization of MNP@mpg-CN

Four hybrid materials based on metallic nanoparticles (MNP; M = Ru or Pt) supported onto mesoporous graphitic carbon nitride (mpg-CN) have been prepared following the organometallic approach (Scheme 1).^{18,20,21} The preparation of the Pt nanoparticles presented in this work has been recently reported by some of the authors.²² Briefly, the metal precursor, either [Ru(cod)(cot)] (cod = 1,5-cyclooctadiene; cot = 1,3,5-cyclooctatriene) or [Pt(dba)₃] (dba = dibenzylideneacetone), was placed in a Fisher-Porter bottle and dissolved in THF in the

presence of mpg-CN, synthesized according to a previously reported procedure.²³ For the in-situ preparation of RuPP NPs onto the surface of mpg-CN (in-RuPPNP@mpg-CN), 4-phenylpyridine (PP) was previously dissolved in the THF solution containing the Ru precursor. Then, the Fisher-Porter reactor was pressurized with three bars of H₂ and left under vigorous stirring for 16 h to yield RuNP@mpg-CN (Ru NPs directly stabilized onto mpg-CN surface), in-RuPPNP@mpg-CN, and PtNP@mpg-CN (Pt NPs directly stabilized onto mpg-CN surface). For the ex-situ preparation of RuPP NPs onto the surface of mpg-CN (ex-RuPPNP@mpg-CN), Ru NPs stabilized with 4-phenylpyridine were initially prepared according to the procedure previously described by some of the authors.¹⁹ Then, these RuPP NPs were impregnated onto mpg-CN.

High-Resolution Transmission electron microscopy (HR-TEM), High-Angle Annular Dark-Field Scanning Transmission Electron Microscopy (HAADF-STEM), Energy-Dispersive X-ray spectroscopy (EDX), Inductively Coupled Plasma Optical Emission Spectrometry (ICP-OES), X-ray Photoelectron Spectroscopy (XPS), nitrogen sorption measurements, and powder X-Ray Diffraction (XRD) experiments have been carried out to characterize the hybrid materials.



Scheme 1. Synthetic procedure for the preparation of MNP@mpg-CN hybrid materials.

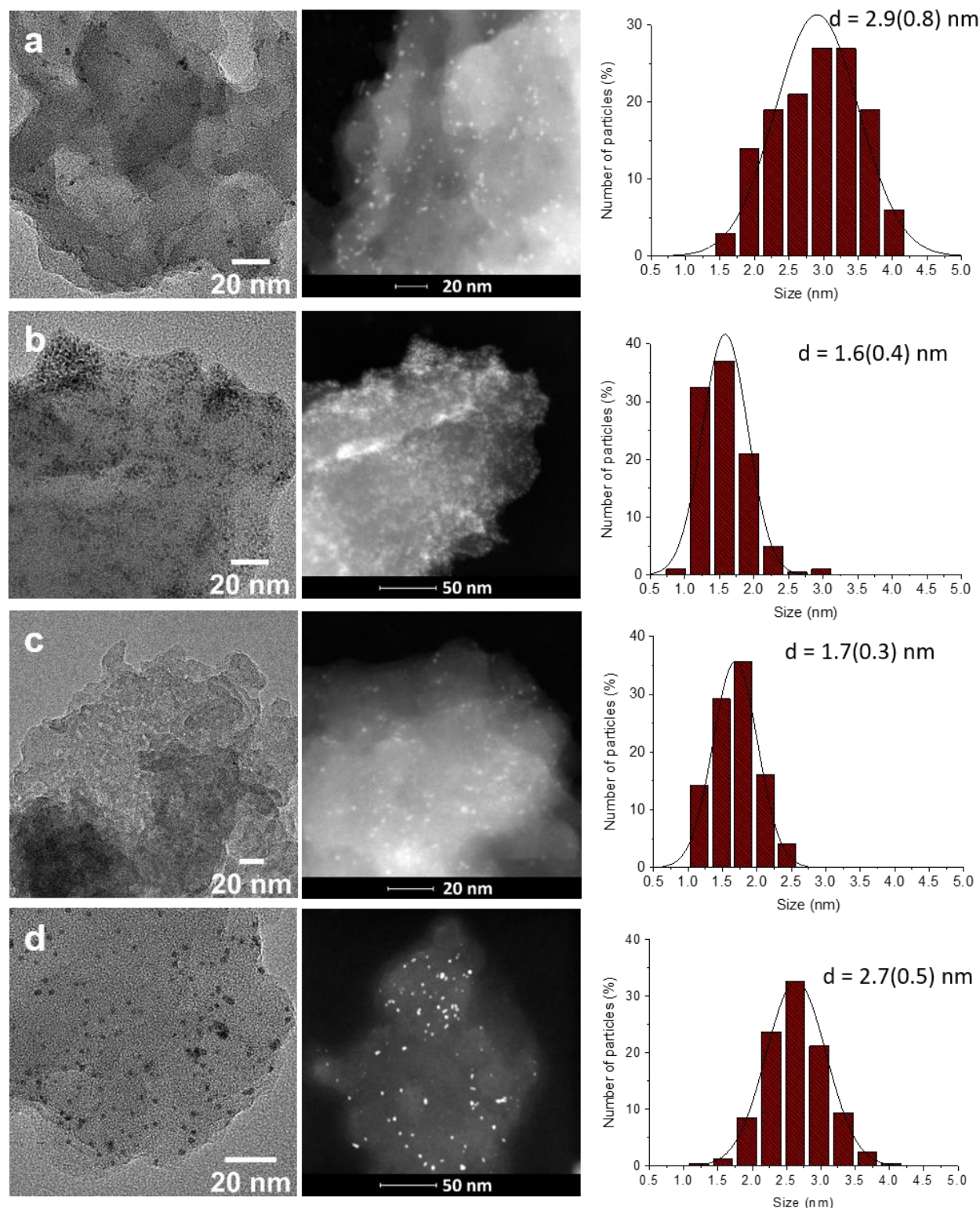


Figure 1. HR-TEM images (left column), high-angle annular dark-field (HAADF)-STEM images (central column) and size distribution (right column) of RuNP@mpg-CN (a), in-RuPPNP@mpg-CN (b), ex-RuPPNP@mpg-CN (c) and PtNP@mpg-CN (d).

For RuNP@mpg-CN and PtNP@mpg-CN, HR-TEM and HAADF-STEM micrographs show the presence of small nanoparticles (NPs), homogeneous in size and shape, and well-distributed all over the mpg-CN (Figure 1a and 1d, for RuNP@mpg-CN and

PtNP@mpg-CN, respectively). The mean size of these nanoparticles is 2.9(0.8) nm for RuNP@mpg-CN and 2.7(0.5) nm for PtNP@mpg-CN. For in-RuPPNP@mpg-CN, the NPs are smaller than those found for RuNP@mpg-CN, as expected

considering the extra stabilization afforded by 4-phenylpyridine ligand (mean size of 1.6(0.4) nm, Figure 1b). However, they are highly aggregated onto the surface of the mpg-CN. This is probably due to the higher affinity of the precursor seeds of the Ru NPs towards 4-phenylpyridine than to the surface of the mpg-CN. Thus, once formed, the NPs can no longer penetrate the pores of the mpg-CN and form aggregates at its surface. In contrast, Ru NPs are not easily distinguishable in the HR-TEM micrographs for ex-RuPPNP@mpg-CN (Figure 1c). This can be explained assuming that the nanoparticles are preferentially deposited inside the pores of the carbon nitride. The HAADF-STEM images confirm this hypothesis showing the presence of isolated, small, and well distributed nanoparticles (mean size of 1.7(0.3) nm) inside the mpg-CN material. The presence of Ru in RuNP@mpg-CN, in-RuPPNP@mpg-CN, and ex-RuPPNP@mpg-CN has been confirmed by EDX analyses (Figure S1). EDX analysis for PtNP@mpg-CN has been reported previously by some of the authors.²² For comparison, in Figure S2, the HR-TEM and HAADF-STEM micrographs of pure mpg-CN are also displayed.

XPS measurements have been recorded to better understand the chemical composition of the NPs. For RuNP@mpg-CN and in-RuPPNP@mpg-CN, a mixture of Ru(0) and Ru(IV) species can be identified when the Ru 3p region is analysed (Ru 3d peaks could not be analysed due to the overlapping with C 1s signals). Figure S3 depicts the Ru 3p_{3/2} signal of RuNP@mpg-CN and in-RuPPNP@mpg-CN. Interestingly, a predominance of Ru(IV) species can be observed for RuNP@mpg-CN, whereas Ru(0) species are dominating in the case of in-RuPPNP@mpg-CN. Unfortunately, the XPS spectrum of ex-RuPPNP@mpg-CN does not show any appreciable peak attributable to Ru. This can be ascribed to the fact that in this sample Ru NPs are deposited deep inside the pores of mpg-CN, as confirmed by HR-TEM and HAADF-STEM micrographs (vide supra). XPS analysis of PtNP@mpg-CN has been reported previously and shows the predominance of Pt(0) species with a small contribution of Pt(II) species.²²

Specific surface areas (S_{BET}) of all samples have been obtained by nitrogen sorption measurements to find out any possible structural modifications of hybrid MNP@mpg-CN samples (Figure S4). Pure mpg-CN displays a specific surface area of 165 m²/g, confirming its mesoporosity. After loading with MNPs, the specific surface area of the hybrid mpg-CN samples decreases, probably due to a partial blocking of the mpg-CN mesopores. The corresponding surface area are 102, 89, 92, and 110 for

RuNP@mpg-CN, in-RuPPNP@mpg-CN, ex-RuPPNP@mpg-CN, and PtNP@mpg-CN, respectively. The average pore size of pure mpg-CN calculated from the BJH analysis is 3.8 nm. For the hybrid materials, an identical value (3.8 nm) is found for RuNP@mpg-CN, in-RuPPNP@mpg-CN, and PtNP@mpg-CN, while it slightly increases to 4.1 nm in the case of ex-RuPPNP@mpg-CN.

Powder X-ray diffraction (XRD) patterns of MNPs@mpg-CN photocatalysts have been recorded and compared to that of pure mpg-CN (Figure S5). The diffractograms of the Ru-containing samples display two peaks at 2 θ values of 13.1° and 27.4°, which confirms that the crystallinity of mpg-CN is maintained after Ru loading. Reflection at 2 θ value of 27.4° can be attributed to the layered stacking and reflection at 13.1° indicates interplanar repetition of tris-triazine units.²⁴ Due to the low Ru loadings, no reflections corresponding to the MNPs have been detected. The diffractogram of PtNP@mpg-CN has been recently reported,²² and also confirms that the crystallinity of mpg-CN is preserved after Pt loading.

The metal content (wt.% Ru or wt.% Pt) present in each of the three samples was quantified through ICP-OES, revealing a metal content of 0.52%, 0.69%, 0.55%, and 1.2% for RuNP@mpg-CN, in-RuPPNP@mpg-CN, ex-RuPPNP@mpg-CN, and PtNP@mpg-CN, respectively (expected values were 0.6% for the Ru-based materials and 1.2% for the Pt one). These values confirm, within the measurement uncertainty, that the organometallic approach can afford a quantitative loading of metallic NPs and, in this case, a similar molar concentration of metal in the samples.

Photocatalytic experiments

The hybrid materials have been tested as catalysts towards the light-driven hydrogen evolution reaction (HER). Even if mpg-CN is thermodynamically able to harvest (sun)light and use photogenerated electrons to reduce protons to hydrogen, it is mandatory to use appropriate co-catalysts (in our case MNPs) to improve the rate of the reaction. The photocatalytic experiments have been carried out for 24 h upon visible light irradiation (>395 nm, 300 W Xe lamp) in the presence of 10% triethanolamine (TEOA) as the sacrificial electron donor. The rate of H₂ produced, measured per g of photocatalyst and hour ($\mu\text{mol}\cdot\text{h}^{-1}\cdot\text{g}^{-1}$), has been determined from the slope of the kinetic traces (Figures S6 and S7). The total amount of H₂ produced (μmol) has been confirmed by gas chromatography.

Table 1. Photocatalytic H₂ evolution using MNP@mpg-CN samples (M = Ru, RuPP or Pt) under visible light irradiation (>395 nm; 24 hrs) using a 300 W Xe lamp.

Entry	Hybrid Material	MNP@mpg-CN (mg)	Metal (μmol)	H ₂ ($\mu\text{mol}\cdot\text{h}^{-1}\cdot\text{g}^{-1}$) ^a	H ₂ (total μmol)	TON ^b (–)	TOF (h ^{–1})
1	mpg-CN	–	–	2	1	–	–
2	RuNP@mpg-CN	26.4	1.36	137	87	64	2.7
3	in-RuPPNP@mpg-CN	25.9	1.77	155	96	54	2.3
4	ex-RuPPNP@mpg-CN	26.6	1.45	129	82	57	2.4
5	PtNP@mpg-CN	25.0	1.54	870	522	339	14.1

^a μmol of H₂ produced per hour and per g of catalyst (MNP@mpg-CN); ^b TON considering the μmol of metal.

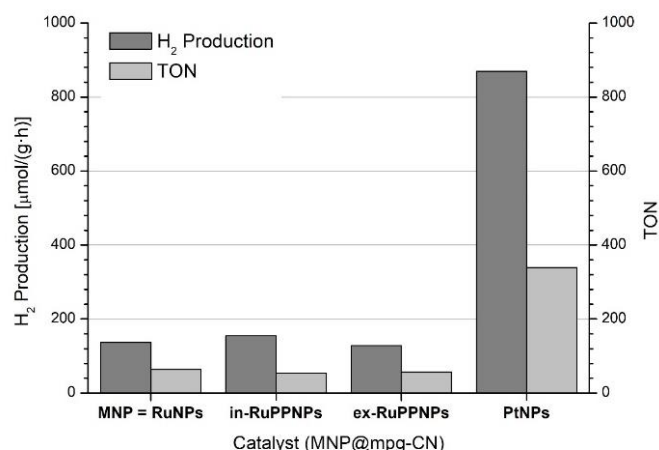


Figure 2. Photocatalytic H₂ evolution of MNP@mpg-CN under visible light irradiation (>395 nm; 24 hrs) using 300 W Xe lamp.

These quantities and the corresponding maximum turnover numbers (TONs) after 24 h (determined considering the total μmol of metal) have also been calculated and can be found in Figure 2 and Table 1.

In all cases, the hybrid photocatalysts do not deactivate during 24 h of H₂ production and their activities (Table 1) can be unambiguously compared using the estimated rates of H₂ production, namely μmol of H₂ per g of photocatalyst and hour. PtNP@mpg-CN (870 μmol·g⁻¹·h⁻¹) clearly outperforms all the Ru samples (137, 155, and 129 μmol·g⁻¹·h⁻¹ for RuNP@mpg-CN, in-RuPPNP@mpg-CN, and ex-RuPPNP@mpg-CN, respectively). Following this trend, PtNP@mp-CN produces more than 5-fold the total amount of H₂ (522 μmol) than any of the Ru samples and the final TON is 339 (Table 1).

The photocatalytic studies on the three different samples containing Ru nanoparticles (Table 1, entries 2, 3 and 4, respectively) show that the total H₂ production after 24 h is similar (87, 96, and 82 μmol of H₂ for RuNP@mpg-CN, in-RuPPNP@mpg-CN, and ex-RuPPNP@mpg-CN, respectively). Notably, this behaviour is also confirmed when the TON values are considered. In this case, the TON for RuNP@mpg-CN (64) is larger than those obtained for in-RuPPNP@mpg-CN (54) and ex-RuPPNP@mpg-CN (57), even if RuPPNPs are smaller and thus present a higher amount of catalytically active sites.

Stability tests.

To prove the stability of the photocatalytic systems, long-term experiments (65 h) were carried out with RuNP@mpg-CN and PtNP@mpg-CN. The experiments were performed in a 6 mL glass cell thermostated at 25 °C upon visible light irradiation (>400 nm, 300 W Xe lamp) of 2.5 mg of the corresponding hybrid material dispersed in 3.8 mL of an aqueous TEOA solution (10%). Figure 3 shows the H₂ evolution kinetics of these experiments. No sign of deactivation can be detected for PtNP@mpg-CN, proving the high stability of the system. In contrast, a decrease of the H₂ production rate is observed for

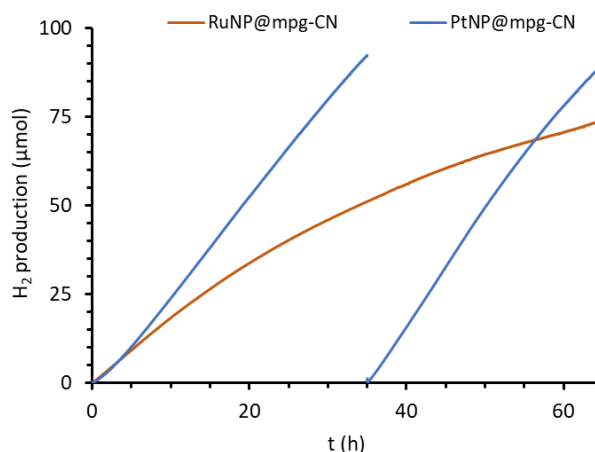


Figure 3. Photocatalytic H₂ evolution with RuNP@mpg-CN and PtNP@mpg-CN in the presence of visible light irradiation (>395 nm) from 300 W Xe lamp using TEOA as the sacrificial electron donor agent with a duration of the photocatalytic reaction of 65 hrs.

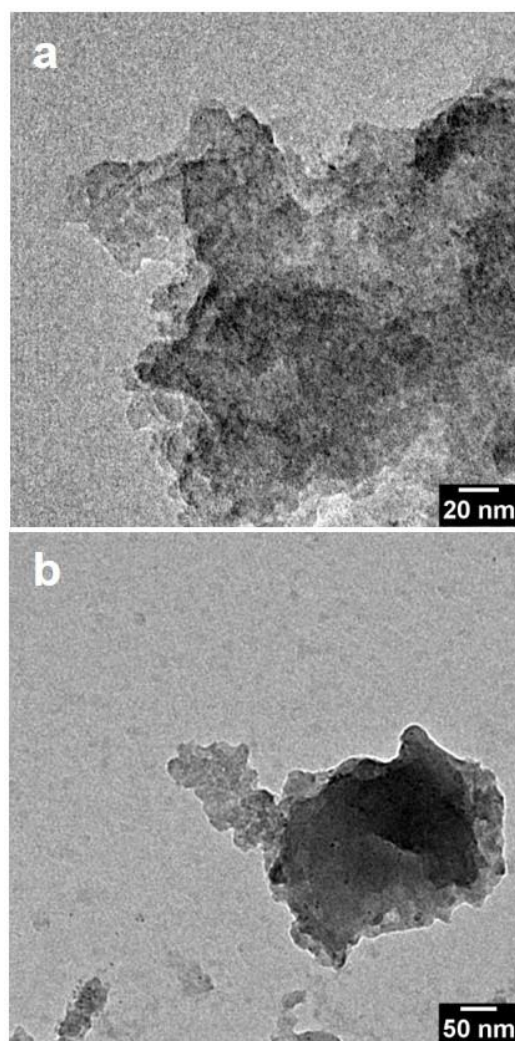


Figure 4. TEM micrographs after the photocatalytic stability tests. a) RuNP@mpg-CN and b) PtNP@mpg-CN.

RuNP@mpg-CN, but the system still remains active after 65 h. ICP-OES analyses of the solutions after the stability tests, show that only 0.06% of Ru was leached from RuNP@mpg-CN and 0.04% from PtNP@mpg-CN, meaning that the loss of activity in the case of RuNP@mpg-CN is probably due to passivation of the surface of the Ru NPs rather than to the detachment of the catalytic NPs from the mpg-CN support. This hypothesis is further confirmed by inspection of the TEM micrographs of the spent photoreaction (Figure 4), in which the MNPs can be still observed onto the surface of the mpg-CN in the case of both RuNP@mpg-CN and PtNP@mpg-CN.

Photophysical experiments.

To elucidate the reasons for the different photocatalytic performances of the hybrid materials tested, photophysical studies on the MNP@mpg-CN samples have been undertaken. The diffuse-reflectance absorption spectrum of mpg-CN is characterized by an intense absorption at wavelengths below 420 nm, assigned to π - π^* transitions, and a tail at longer wavelengths, attributed to n - π^* transitions^{25,26}. Tauc plot analysis (Figure S8) provides a bandgap energy of ca 2.7 eV, in agreement with literature data.²⁷ Excitation of mpg-CN at 390 nm in water induces a broad luminescence with a maximum at 475 nm (Figure S9). The time-resolved emission decay of mpg-CN has been then measured by TC-SPC (excitation at 380 nm, analysis at 470 nm). The decay (Figure S10) can be fitted using a tri-exponential function leading to three time-components of $\tau_1 = 0.75$ ns, $\tau_2 = 3.28$ ns, and $\tau_3 = 14.92$ ns, corresponding to an amplitude-weighted average lifetime of $\langle \tau \rangle = 2.04$ ns.

In the absence of the TEOA sacrificial donor, all the samples display comparable emission lifetimes of ca 2 ns (see Table S1, only a slight decrease is observed in the case of PtNP@mpg-CN and ex-RuPPNP@mpg-CN) suggesting that the attached catalyst quenches the emissive states with low efficiency (<14%). In the presence of TEOA, a slight decrease in the lifetime can be observed in all cases, corresponding to hole transfer efficiencies between 4-7%. Overall, the weak extent of luminescence quenching by both the metal nanoparticles and TEOA donor suggests that both electron transfer to the catalyst and hole transfer to the sacrificial agent are not much efficient from the emissive states, i.e., those states corresponding to electrons and holes close to the band edges.

A major decay pathway of charge carriers in mpg-CN is indeed expected to involve progressive trapping into deep trap levels. The corresponding electronic states are usually non-emissive and can be conveniently followed by transient absorption spectroscopy.^{27,28} Excitation of mpg-CN at 355 nm gives a transient signal in the μ s-to-ms timescale featuring a maximum at ca 750 nm (Figure S11a). As reported earlier,^{27,29,30} this transient signature can be assigned to photogenerated charge carriers, primarily trapped electrons.²⁷ In the presence of 10% TEOA, a similar transient signal is observed, which, however, displays increased amplitude and longer lifetime (Figure S11). This result can be explained considering that TEOA efficiently reacts with trapped holes in the ns- μ s time scale (i.e., in the time window below the resolution of the experiment) leaving long-

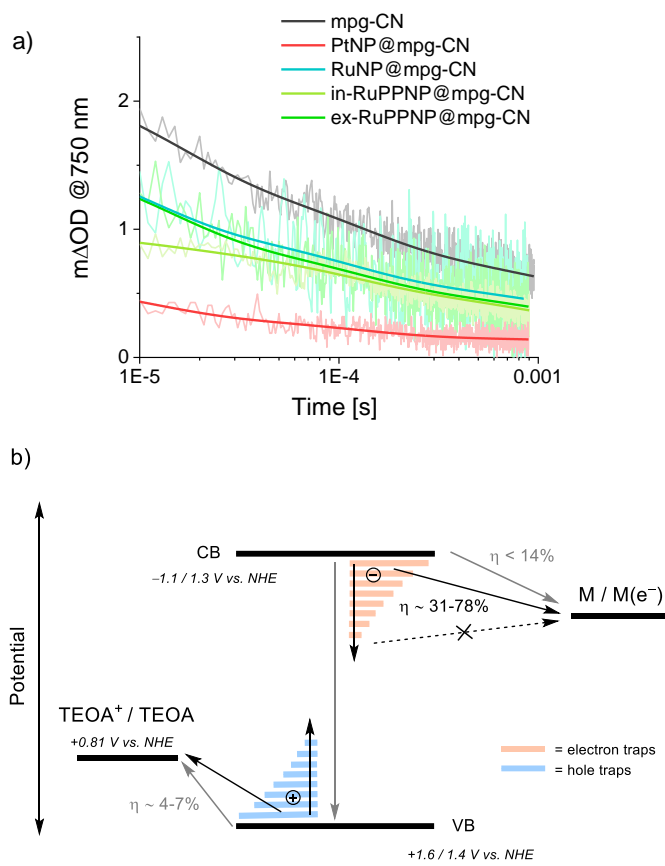


Figure 5. a) Single wavelength kinetics at 750 nm obtained by laser flash photolysis (excitation at 355 nm, isoabsorbing samples) of mpg-CN, PtNP@mpg-CN, RuNP@mpg-CN, in-RuPPNP@mpg-CN, and ex-RuPPNP@mpg-CN in water in the presence of 10% TEOA; b) schematic representation of the main photoinduced processes involving both charge carriers in emissive states (grey arrows) and trapped charge carriers in non-emissive states (black arrows) with corresponding efficiencies (where known); potentials of CB and VB of mpg-CN, and TEOA have been taken from literature.

lived electrons which decay with complex kinetics, associated to trapping-detrapping processes.³¹ Single wavelength kinetic analysis at 750 nm, obtained on isoabsorbing samples at the excitation wavelength, was then used to check the fate of the photogenerated electrons in the presence of the metal nanoparticles. The results are reported in Figure 5a. Notably, the kinetics of the transient decay is apparently unaffected by the presence of the catalyst.[‡] However, the amplitude of the transient signal (prompt Δ OD at ca 10 μ s) is apparently quenched in the presence of the nanoparticles suggesting that trapped electrons can be transferred to the catalytic metal within a comparable timescale of the hole-scavenging by the donor, namely in the ns- μ s time window. This behaviour is comparable to that documented for the photoinduced electron transfer from carbon nitride to electron scavengers such as Ag^+ ions.²⁷ Interestingly, the amount of prompt transient quenching varies depending on the nature of the metal nanoparticles in the order PtNP@mpg-CN (78%) \gg in-RuPPNP@mpg-CN (48%) $>$ ex-RuPPNP@mpg-CN (32%) \sim RuNP@mpg-CN (31%).[§] A summary of the photophysical results is schematically depicted in Figure 5b.^{28,30,32–34}

Discussion

Four hybrid MNPs@mpg-CN (M = Ru or Pt) photocatalysts have been prepared through the organometallic approach and tested in the light-driven hydrogen evolution reaction (HER). First, Ru and Pt NPs have been directly synthesized onto the surface of mpg-CN without any further stabilization leading to PtNP@mpg-CN and RuNP@mpg-CN samples. These procedures yield homogeneous and well-dispersed NPs. For Ru, the same reaction conditions have been also used with the addition of 4-phenylpyridine (PP) as an extra stabilizer, yielding smaller but aggregated NPs (in-RuPPNP@mpg-CN). This is probably due to the higher affinity of the NPs towards PP ligand than towards the surface of mpg-CN. Finally, Ru NPs have been synthesized ex-situ, stabilized by PP ligand, and then impregnated onto the surface of the mpg-CN (ex-RuPPNP@mpg-CN). The photocatalytic activity of all the samples has been tested towards the HER. The Pt-containing hybrid material clearly outperforms all the Ru counterparts and the performance of the different samples has been compared in terms of rate of H₂ production leading to values of 870, 137, 155, and 129 $\mu\text{mol}\cdot\text{h}^{-1}\cdot\text{g}^{-1}$ for PtNP@mpg-CN, RuNP@mpg-CN, in-RuPPNP@mpg-CN, and ex-RuPPNP@mpg-CN, respectively (see Table 1).

Photophysical studies have been employed to rationalize the trend in photosynthetic activity. As a matter of fact, an intriguing comparison can be made between the hydrogen evolution rates and the amount of quenching of the transient signal associated to photogenerated trapped electrons (Figure 3a). This latter can be indeed correlated to the efficiency of the reduction of the metal catalyst by trapped electrons in the mpg-CN. Interestingly, this experimental trend appreciably parallels the observed photochemical hydrogen evolution activity (i.e., the trend in H₂ production rates), clearly suggesting that electron transfer from the photoexcited carbon nitride to the catalyst might represent the rate determining step in hydrogen evolution photocatalysis by MNP@mpg-CN. In this respect, the improved performance of the PtNP@mpg-CN over all Ru-based materials arises from improved electron transfer yields (78% vs. 31–48% for the Pt- and Ru-based systems, respectively). An intrinsic inertness of RuNPs towards electron transfer has been already observed in light-triggered hydrogen evolution when attached to sensitized TiO₂.³⁵

The photophysical experiments point out some further interesting differences, particularly when the ruthenium-based hybrid samples are compared. As a matter of fact, a larger electron transfer yield has been observed in the case of in-RuPPNP@mpg-CN than both ex-RuPPNP@mpg-CN and RuNP@mpg-CN (48% vs 31–32%, respectively, Figure 3b). The reason for this experimental observation possibly resides on the larger amount of active surface sites due to the reduced size of the nanoparticles, when in-RuPPNP@mpg-CN and RuNP@mpg-CN are compared, and to slightly improved interactions between the photoactive mpg-CN and the catalytic nanoparticles, when confronting in-RuPPNP@mpg-CN and ex-RuPPNP@mpg-CN. Thus, the photophysical experiments highlight the importance of the 4-phenylpyridine ligands that act as stabilizing agents on the surface of the nanoparticles to

enhance the electron transfer rate between the photosensitizing unit and the nanocatalysts. This is consistent with the recent observation that stabilization with 4-phenylpyridine definitely enhances the electrocatalytic performance of RuNPs.¹⁹ However, the observation of comparable photocatalytic activity among the Ru-samples (with only a small improvement in terms of hydrogen evolution rates in the case of in-RuPPNP@mpg-CN than both RuNP@mpg-CN and ex-RuPPNP@mpg-CN, see above) strongly suggests that, although the efficiency of the light-triggered electron transfer to the catalyst has a pivotal role in determining the overall H₂ production yield, the morphology of the nanomaterial has an important impact as well. In this respect, the partial aggregation found for in-RuPPNP@mpg-CN might be somewhat detrimental towards H₂ production due to a non-ideal connectivity between the catalytic Ru NPs and the light-harvesting mpg-CN. Thus, the profitable exploitation of the inherent kinetic advantages of RuNPs stabilized by 4-phenylpyridine ligands to challenge the performance of Pt-based systems possibly requires a further specific control of the 3D structure of the hybrid photocatalyst. In this respect, strategies to better stabilize RuNPs on semiconducting heterogeneous sensitizers are currently planned in our labs.

Experimental Section

General procedure and reagents.

The handling of reagents and the synthesis of materials has been carried out under inert conditions, either in a glovebox (MBRAUN Unilab) under argon or using Schlenk-line and Fischer–Porter bottle techniques. Glassware was dried before use at 120 °C in the oven. The following chemicals were used as purchased: [Ru(cod)(cot)] from NanoMePS, [Pt(dba)₃] from Strem Chemicals, 4-phenylpyridine (PP) and triethanolamine (TEOA) from Sigma-Aldrich, and hydrogen (H₂) gas from Abelló Linde (>99,999%). Mesoporous graphitic carbon nitride (mpg-CN) was prepared as indicated in the next section. Both solvents, tetrahydrofuran (THF) and hexane, purchased in Scharlab, were first dried and distilled and then degassed via freeze–pump–thaw cycles.

Synthesis of mesoporous graphitic carbon nitride (mpg-CN).

For the preparation of mpg-CN, whose synthesis was previously reported by some authors of this article,²³ cyanamide and triethylorthosilicate are used as precursors, obtaining a mixture of carbon nitride and silica, which is treated with NH₄HF₂, thus eliminating the SiO₂ and producing the sought mpg-CN.

Synthesis of MNP@mpg-CN (M = Ru or Pt) and in-RuPPNP@mpg-CN.

200 mg of mpg-CN were placed into a Fischer–Porter bottle. The reactor was connected to the Schlenk line, where a heat gun was used for a few minutes to dry the system, and then allowed to cool to room temperature. Inside the glovebox, 3.9 mg / 0.013 mmol of [Ru(cod)(cot)] (for RuNP@mpg-CN and for in-RuPPNP@mpg-CN) or 11.3 mg / 0.013 mmol of [Pt(dba)₃] (for

PtNP@mpg-CN) were weighted and put into the reactor. After that, 16 mL of THF were added (for in-RuPPNP@mpgCN, 0.4 mg / 0.003 mmol of 4-phenylpyridine are dissolved in the solvent). Then, 3 bars of H₂ were used to pressurize the reactor at room temperature, and the reaction was kept under vigorous magnetic stirring overnight (16 h). The hydrogen pressure is then removed. Before recovering the material, a TEM sample was prepared by dropping a small aliquot of the reaction mixture onto a carbon-coated copper grid (400 mesh). Finally, the hybrid materials were isolated by centrifugation, cleaned with hexane, and dried under vacuum.

Synthesis of ex-RuPPNP@mpg-CN.

A suspension of RuPP NPs was prepared in THF starting from 3.9 mg / 0.013 mmol of [Ru(cod)(cot)] and 0.4 mg / 0.003 mmol of 4-phenylpyridine and following a procedure previously described.¹⁹ Then, 200 mg of mpg-CN were added to the suspension of RuPP NPs in THF and left stirring for 24 h. After that, a TEM sample was prepared by dropping a small aliquot of the reaction mixture onto a carbon-coated copper grid (400 mesh). Finally, the hybrid material was isolated by centrifugation, cleaned with hexane, and dried under vacuum.

Characterization.

Transmission Electron Microscopy (TEM) and Energy-Dispersive X-ray spectroscopy (EDX). Transmission Electron Microscopy (TEM) and Energy-Dispersive X-ray spectroscopy (EDX) analyses were performed at the Servei de Microscopia de la UAB with a JEOL JEM 2011 electron microscope working at 200 kV with a resolution point of 2.5 Å, equipped with a Detector EDS Oxford Instruments X-max (136 eV energy resolution). Mean size and size distributions of the Pt and Ru NPs were determined by manually measuring at least 200 particles, using ImageJ freeware to process the obtained TEM micrographs.

High-Resolution Transmission Electron Microscopy (HR-TEM) and High-Angle Annular Dark-Field Scanning Transmission Electron Microscopy (HAADF-STEM). High-resolution transmission electron microscopy (HR-TEM) and HAADF-STEM images were acquired at the Electron Microscopy Unit of the Institut Català de Nanociència i Nanotecnologia (ICN2, Barcelona, Spain) using a FEI Tecnai G2 F20 microscope operated at 200 kV.

X-ray Photoelectron Spectroscopy (XPS). The chemical composition of the photocatalysts were investigated using XPS, which was performed in an equipment located at Institut Català de Nanociència i Nanotecnologia (ICN2, Barcelona, Spain), with a Phoibos 150 analyzer (SPECS GmbH, Berlin, Germany) in ultra-high vacuum conditions (base pressure 5·10⁻¹⁰ mbar) with a monochromatic aluminum K_α X-ray source (1486.74 eV). The energy resolution measured by the FWHM of the Ag 3d_{5/2} peak for a sputtered silver foil was 0.62 eV.

Specific Surface Area (S_{BET}). The surface area was measured on a Quantachrome Autosorb-1 apparatus. Nitrogen adsorption-desorption isotherms were measured at 77.3 K after degassing the samples at 120 °C for 6 h. Specific surface areas were

determined through the Brunauer-Emmett-Teller (BET) method.

X-ray Powder Diffraction (XRD). The XRD patterns were measured in Bruker AXS D8 advanced diffractometer equipped with a position sensitive detector (PSD) and a curved germanium (111) primary monochromator and the radiation used was Cu-K_α (λ = 1.5418 Å).

Inductively coupled plasma optical emission spectrometry (ICP-OES). Quantification of Pt and Ru, expressed in (wt%), was carried out at Servei d'Anàlisi Química (SAQ), in the Universitat Autònoma de Barcelona, Spain, employing an inductively coupled plasma optical emission spectrometry (ICP-OES) Agilent Optima 5900 instrument.

Photocatalytic tests. 25 mg of photocatalyst were placed into the reactor (total volume of the reactor 51.3 mL). The reactor was then sealed with quartz glass. The reactor is connected to a Schlenk-Line apparatus (argon/vacuum). After the reactor was evacuated, 38 mL of an aqueous solution with 10 vol.% triethanolamine (TEOA) as the sacrificial reagent, which was previously flushed with argon for 20 minutes, was added with a syringe through a tap at the head of the reactor with an argon counter current. The reaction mixture was irradiated with a 300 W Xenon lamp (L.O.T. Oriel QuantumDesign, Germany, with a 395 nm filter) under constant stirring for 24 h. The temperature was held constant at 30 °C by using a thermostat (LAUDA ECO RE 630). The distance from the lamp to the reactor was 10 cm. The pressure curve in the reactor was measured with a pressure sensor (Type-P30, Δp = ±0.1, WIKA Alexander Wiegand SE & Co. KG, Germany). At a constant temperature of the reaction mixture, the amount of hydrogen produced can be determined with the ideal gas equation.³⁶ In addition, the hydrogen content was determined by gas chromatography. For that, 8 mL of the gas in the headspace was taken with a syringe, which had been previously flushed with argon. The hydrogen content in the gas volume was measured with two injections of 4 mL each in a gas chromatograph (GC Agilent 7890 A) equipped with a Thermal Conductivity Detector (TCD). The gas sample was manually injected into the gas chromatograph. The column in the GC consists of Carboxen 1000 and argon was used as the carrier gas.

Stability Tests. The hydrogen evolved was measured by using a Clark hydrogen electrode (Unisense H2-NP-9463). The photocatalytic hydrogen evolution reaction was performed in a 6 mL glass cell thermostated at 25 °C, containing 3.8 mL of 10% TEOA as the SED in which the photocatalyst was dispersed by stirring. The solution was degassed with Ar bubbling for at least 10 min until stabilization of the signal. A flat signal was recorded for at least 2 min. Then, the cell was irradiated with a solar simulator (Abet 10 500) containing a Xe lamp placed at exactly 1 sun (100 mW·cm⁻²) distance. The cell was sealed with a septum and grease and the Clark electrode tip was introduced into the headspace of the cell to measure the H₂ formed. Dissolved H₂ was neglected due to its low solubility in aqueous solution. After recording the hydrogen evolution, the cell was degassed by Ar

bubbling and calibration was performed by injecting known volumes of H₂ (usually 50, 100, 150, 200, 250, 300 and 400 μ L) with a gas-tight Hamilton syringe.

Photophysical experiments. Absorption spectra in the diffuse-reflectance mode were obtained on a Jasco V-570 spectrophotometer using an integrating sphere setup. Steady-state luminescence was measured on an Edinburgh Instrument spectrofluorometer. Time-resolved emission measurements were obtained using a TC-SPC apparatus (PicoQuant PicoHarp 300) equipped with a sub-nanosecond LED source (380 nm, 500–700 ps pulse width) powered by a PicoQuant PDL 800-B variable (2.5–40 MHz) pulsed power supply. The decays were analysed using a PicoQuant FluoFit Global Fluorescence Decay Analysis Software. Transient absorption measurements were performed with a custom laser spectrometer comprised of a Continuum Surelite II Nd:YAG laser (FWHM 6 – 8 ns) with frequency tripled (355 nm) option, an Applied Photophysics xenon light source including a mod. 720 150W lamp housing, a mod. 620 power-controlled lamp supply and a mod. 03 –102 arc lamp pulser. Laser excitation was provided at 90° with respect to the white light probe beam. Light transmitted by the sample was focused onto the entrance slit of a 300 mm focal length Acton SpectraPro 2300i triple grating, flat field, and double exit monochromator equipped with a photomultiplier detector (Hamamatsu R3896). Signals from the photomultiplier were processed using a TeledyneLeCroy 604Zi (400 MHz, 20 GS/s) digital oscilloscope. The excitation pulse (355 nm wavelength) was defocused using a diverging lens and set to an average energy of \sim 5 mJ/pulse using a combination of neutral density filters (Edmund Optics).

Conclusions

Hybrid materials have been obtained by coupling mpg-CN with Pt and Ru nanoparticles prepared using the organometallic approach. Three different Ru-based samples have been considered which differ on the presence/absence of 4-phenylpyridine as the stabilizing agent and the *in-situ* or *ex-situ* integration of the Ru nanoparticles with the mpg-CN. The photocatalytic activity towards the HER has been examined in aqueous solution using TEOA as a sacrificial electron donor. The Pt-based material displays the best performance over all the Ru-based systems as well as improved stability upon prolonged irradiation tests. The trend in photocatalytic activity has been rationalized employing photophysical experiments and related to the different electron transfer efficiencies from the mpg-CN to the metal nanoparticles that follow the order PtNP@mpg-CN \gg in-RuPPNP@mpg-CN $>$ ex-RuPPNP@mpg-CN \approx RuNP@mpg-CN. As to the comparison among Ru-based samples, although improved electron transfer yields are observed for in-RuPPNP@mpg-CN than both ex-RuPPNP@mpg-CN and RuNP@mpg-CN, no net improvement in H₂ production performance is observed, likely ascribable to a non-optimal morphology of the hybrid material. Hence, the light-driven hydrogen production efficiency of hybrid MNPs@mpg-CN

materials strongly depends on a complex interplay among several factors, including electron transfer kinetics, amount of active surface sites, and connectivity between the light-harvesting and catalytic units. The identification, from a structural standpoint, of an optimum combination between semiconducting sensitizers and ruthenium-based catalysts thus represents a great challenge towards the preparation of Pt-free hybrid photosystems.

Author Contributions

M.N., J.G.-A. and M.T. conceived the idea; I.A.-P., A.-D.N., N.R., E.B., L.E., A.A., A.T., M.S., R.S., X.S., M.N., J.G.-A. and M.T. contributed to experimental design; I.A.-P., A.-D.N., N.R., H.H., E.B., A.A., M.N. and J.G.-A performed the experiments and analysed data; I.A.-P., A.-D.N., N.R., E.B., L.E., A.A., A.T., M.S., R.S., X.S., M.N., J.G.-A. and M.T reviewed the data and prepared the manuscript.

Conflicts of interest

There are no conflicts to declare.

Acknowledgements

This project was funded by the Federal Ministry of Education and Research of Germany through the “CO₂ – WIN initiative” under grant number 033RC024A and Deutsche Forschungsgemeinschaft (DFG, German Research Foundation) under Germany’s Excellence Strategy – EXC 2008/1 (UniSysCat) – 390540038. Support from MINECO (PID2019-104171RB-I00) is gratefully acknowledged. I A.-P. acknowledges the Universitat Autònoma de Barcelona for his pre-doctoral grant. J.G.-A. acknowledges Serra Húnter Program. The authors thank the Microscopy Service of the Universitat Autònoma de Barcelona for technical assistance with TEM and SEM. M. N. acknowledges the University of Ferrara for funding (FAR2020) and Mr. Marco Carosino (University of Ferrara) for assistance.

Notes and references

‡ A tri-exponential function with lifetimes in the order of $\tau_1 \sim 10^{-5}$ s, $\tau_2 \sim 10^{-4}$ s, and $\tau_3 \sim 10^{-3}$ s has been used to fit the kinetic traces in all cases. Considering the trapping - detrapping mechanism associated to the decay of the photogenerated charge carriers,²⁸ a power law exponential decay would be much more appropriate. However, since the decaying kinetics has been discussed in detail in previous works¹⁹ and is not of specific interest in the present analysis, we preferred the use of a simpler kinetic treatment.

§ The abatement of the transient signal is not quantitative even in the case of Pt, confirming that electron transfer to the metal nanoparticles always occurs in competition with further trapping. Also, the decaying kinetics appears to be almost independent of the metal nanoparticles, suggesting that progressively trapped electrons lose their energy and do not have sufficient driving force to reduce the metal nanoparticles regardless of the nature of the latter.²⁷

- 1 N. S. Lewis, *Science*, 2016, **351**, aad1920.
- 2 R. Eisenberg, H. B. Gray and G. W. Crabtree, *Proc. Natl.*

- 3 *Acad. Sci. U. S. A.*, 2020, **117**, 12543–12549.
- 3 J. Qi, W. Zhang and R. Cao, *Adv. Energy Mater.*, 2018, **8**, 1701620.
- 4 W. T. Eckenhoff, *Coord. Chem. Rev.*, 2018, **373**, 295–316.
- 5 M. Kondo, H. Tatewaki and S. Masaoka, *Chem. Soc. Rev.*, 2021, **50**, 6790–6831.
- 6 T. Hisatomi, J. Kubota and K. Domen, *Chem. Soc. Rev.*, 2014, **43**, 7520–7535.
- 7 A. Agosti, M. Natali, L. Amirav and G. Bergamini, *ChemSusChem*, 2020, **13**, 4894–4899.
- 8 T. Uekert, C. M. Pichler, T. Schubert and E. Reisner, *Nat. Sustain.*, 2021, **4**, 383–391.
- 9 C. H. Ng, S. H. Teo, N. Mansir, A. Islam, C. G. Joseph, S. Hayase and Y. H. Taufiq-Yap, *Sustain. Energy Fuels*, 2021, **5**, 4457–4511.
- 10 J. Zhang, Y. Chen and X. Wang, *Energy Environ. Sci.*, 2015, **8**, 3092–3108.
- 11 Q. Zhu, Z. Xu, B. Qiu, M. Xing, J. Zhang, Q. Zhu, Z. Xu, M. Xing, J. Zhang and B. Qiu, *Small*, 2021, **17**, 2101070.
- 12 Y. Shiraishi, Y. Kofuji, S. Kanazawa, H. Sakamoto, S. Ichikawa, S. Tanaka and T. Hirai, *Chem. Commun.*, 2014, **50**, 15255–15258.
- 13 P. An, W. Zhu, L. Qiao, S. Sun, Y. Xu, D. Jiang, M. Chen and S. Meng, *Dalt. Trans.*, 2021, **50**, 2414–2425.
- 14 A. Eftekhari, *Int. J. Hydrogen Energy*, 2017, **42**, 11053–11077.
- 15 N. Romero, R. Bofill, L. Francàs, J. García-Antón and X. Sala, *Catal. 2021, Vol. 11, Page 754*, 2021, **11**, 754.
- 16 C. C. L. McCrory, S. Jung, I. M. Ferrer, S. M. Chatman, J. C. Peters and T. F. Jaramillo, *J. Am. Chem. Soc.*, 2015, **137**, 4347–4357.
- 17 J. Creus, J. De Tovar, N. Romero, J. García-Antón, K. Philippot, R. Bofill and X. Sala, *ChemSusChem*, 2019, **12**, 2493–2514.
- 18 C. Amiens, D. Ciuculescu-Pradines and K. Philippot, *Coord. Chem. Rev.*, 2016, **308**, 409–432.
- 19 J. Creus, S. Drouet, S. Suriñach, P. Lecante, V. Collière, R. Poteau, K. Philippot, J. García-Antón and X. Sala, *ACS Catal.*, 2018, **8**, 11094–11102.
- 20 I. Álvarez-Prada, D. Peral, M. Song, J. Muñoz, N. Romero, L. Escriche, A. Acharjya, A. Thomas, R. Schomäcker, M. Schwarze, X. Sala, M. Tasbihi and J. García-Antón, *Renew. Energy*, 2021, **168**, 668–675.
- 21 J. Muñoz, I. Álvarez-Prada, E. Lopez-Lopez, L. Escriche, N. Romero, X. Sala, M. Mas-Torrent and J. García-Antón, *Sensors Actuators, B Chem.*, 2020, **305**, 127467.
- 22 M. Tasbihi, F. Fresno, I. Álvarez-Prada, A. Acharjya, A. Thomas, L. Escriche, N. Romero, X. Sala, V. A. de la Peña O’Shea and J. García-Antón, *J. CO₂ Util.*, 2021, **50**, 101574.
- 23 K. Kailasam, J. D. Epping, A. Thomas, S. Losse and H. Junge, *Energy Environ. Sci.*, 2011, **4**, 4668.
- 24 M. Tasbihi, A. Acharjya, A. Thomas, M. Reli, N. Ambrožová, K. Koččí and R. Schomäcker, *J. Nanosci. Nanotechnol.*, 2018, **18**, 5636–5644.
- 25 M. Deifallah, P. F. McMillan and F. Corà, *J. Phys. Chem. C*, 2008, **112**, 5447–5453.
- 26 A. B. Jorge, D. J. Martin, M. T. S. Dhanoa, A. S. Rahman, N. Makwana, J. Tang, A. Sella, F. Corà, S. Firth, J. A. Darr and P. F. McMillan, *J. Phys. Chem. C*, 2013, **117**, 7178–7185.
- 27 R. Godin, Y. Wang, M. A. Zwijnenburg, J. Tang and J. R. Durrant, *J. Am. Chem. Soc.*, 2017, **139**, 5216–5224.
- 28 J. J. Walsh, C. Jiang, J. Tang and A. J. Cowan, *Phys. Chem. Chem. Phys.*, 2016, **18**, 24825–24829.
- 29 C. Ye, J. X. Li, Z. J. Li, X. B. Li, X. B. Fan, L. P. Zhang, B. Chen, C. H. Tung and L. Z. Wu, *ACS Catal.*, 2015, **5**, 6973–6979.
- 30 R. Kuriki, H. Matsunaga, T. Nakashima, K. Wada, A. Yamakata, O. Ishitani and K. Maeda, *J. Am. Chem. Soc.*, 2016, **138**, 5159–5170.
- 31 J. Nelson, *Phys. Rev. B - Condens. Matter Mater. Phys.*, 2003, **67**, 1–10.
- 32 Y. Cui, Z. Ding, P. Liu, M. Antonietti, X. Fu and X. Wang, *Phys. Chem. Chem. Phys.*, 2012, **14**, 1455–1462.
- 33 K. Kalyanasundaram, J. Kiwi and M. Graetzel, *Helv. Chim. Acta*, 1978, **61**, 2720–2730.
- 34 Y. Pellegrin and F. Odobel, *Comptes Rendus Chim.*, 2017, **20**, 283–295.
- 35 N. Romero, R. B. Guerra, L. Gil, S. Drouet, I. Salmeron-Sánchez, O. Illa, K. Philippot, M. Natali, J. García-Antón and X. Sala, *Sustain. Energy Fuels*, 2020, **4**, 4170–4178.
- 36 M. Schwarze, D. Stellmach, M. Schröder, K. Kailasam, R. Reske, A. Thomas and R. Schomäcker, *Phys. Chem. Chem. Phys.*, 2013, **15**, 3466–3472.